Shell model studies of nuclei with $A=92$–98

Chang-hua Zhang,[1,2] Shun-jin Wang,[1,2] and Jin-nan Gu[3]
[1]*Center of Theoretical Nuclear Physics, National Heavy Ion Accelerator Laboratory, Lanzhou 730000, People's Republic of China*
[2]*Modern Physics Department, Lanzhou University, Lanzhou 730000, People's Republic of China*
[3]*Institute of Modern Physics, Academia Sinica, Lanzhou 730000, People's Republic of China*

(Received 14 December 1998; published 14 October 1999)

Shell model calculations are carried out for the spectra of nuclei with $92\leqslant A\leqslant 98$ in the model space in which the valence protons occupy the $1f_{5/2}$, $2p_{3/2}$, $2p_{1/2}$, and $1g_{9/2}$ orbitals, and valence neutrons occupy $1g_{9/2}$, $2p_{1/2}$, $2d_{5/2}$, $2d_{3/2}$, $3s_{1/2}$, and $1g_{7/2}$ orbitals using a partition truncation method. We first select partitions that are big enough to describe the spectra of nuclei with $N=50$. Then we combine all possible valence neutron partitions with the selected valence proton partitions of the corresponding nuclei with $N=50$ to diagonalize the Hamiltonians for the nuclei with $54\geqslant N\geqslant 51$. The weak-coupling scheme is used to analyze the experimental data and the calculated results. The concepts of independent nucleon-pair motion in even-even nuclei and the homologous state structure in even-odd nuclei are held in this mass region. The spectra of $^{95}_{42}\mathrm{Mo}_{53}$ and $^{95}_{43}\mathrm{Tc}_{52}$ share a special similar structure; i.e., the low-lying states of $^{95}_{42}\mathrm{Mo}_{53}$ up to 2.5 MeV can be obtained by replacing the last odd proton in $^{95}_{43}\mathrm{Tc}_{52}$ and vice versa. [S0556-2813(99)01611-8]

PACS number(s): 21.60.Cs, 21.10.Jx, 21.10.Pc, 27.60.+j

I. INTRODUCTION

The nuclear shell model has been very successfully used to calculate the properties of light nuclei, such as binding energies, energy levels, etc., in full $\hbar\omega$ model space. As for the more massive nuclei, the shell model has been mostly applied to nuclei around the double-closed or quasi-double-closed core because of the very large model space. For example, the properties of nuclei with $N=50$ in the $A\sim 100$ mass region have been well described in terms of the shell model [1–5] using ^{88}Sr or ^{78}Ni as a core. Shell model studies also have been extended to nuclei with $N<50$ [6–9]. Most of these studies were carried out in $(1g_{9/2},2p_{1/2})$ model space where the calculation was easy to perform. Sinathas *et al.* [10] extended the model space to ($1g_{9/2}$, $2p_{1/2}$, $1f_{5/2}$, and $2p_{3/2}$) to examine nuclei with $N=48$–50. Ghugre *et al.* [11] investigated both the low-lying and high-spin states in some $N=50$ isotones in an even larger model space $\pi(1f_{5/2},2p_{3/2},2p_{1/2},1g_{9/2})$ and ν $(1g_{9/2},2p_{1/2},2d_{5/2},d_{3/2},3s_{1/2})$. The high-spin states of some nuclei with $N>50$ have been established and calculated by Kharraja *et al.* [12]. The large model space calculations for $N=50$ nuclei and more massive $N>50$ nuclei are more difficult than those with the small model calculation. The truncation of configuration space is not a trivial problem in calculations for massive nuclei. Horoi *et al.* [13] ordered the unperturbed approximate energies of the basis states and selected out those whose energies were in the energy window when they studied the massive fp-shell nuclei. Ghugre *et al.* [11] used the partition truncating method when they studied the high-spin states for $N=50$ nuclei. In this paper, we are concerned with nuclei with $40\leqslant Z\leqslant 46$ and $54\geqslant N\geqslant 50$ in the model space used by Ghugre *et al.* [11]. The main interest in this paper is two points: (1) to find a suitable truncation scheme for these nuclei and (2) to investigate the validity of the weak-coupling scheme for these nuclei. As we have shown, the weak-coupling scheme gives a simple explanation of the nuclear structure of the multipole high-excited states in ^{206}Pb induced in the reaction $^{209}\mathrm{Bi}(\vec{p},\alpha)^{206}\mathrm{Pb}$ [14] and of the above ^{146}Gd nuclei [15]. Experiments show that the high-excited states in some nuclei with $A\sim 90$ also display the feature of weak coupling [16]. One may expect that the weak-coupling scheme is quite valid for midheavy and heavy nuclei due to (1) the short range of the nuclear force, which gives a reasonable explanation why the modified surface delta interaction is quite successfully used in the $A\sim 208$ mass region; (2) for midheavy and heavy nuclei, there is a intruder single-particle state with high angular momentum and opposite parity and the like-particle pairs occupying such intruder state interact weakly and can be approximately treated as independent motion bosons; the residual interaction between valence particles occupying the intruder state and other states is also very weak [15]; (3) the valence protons and neutrons occupy two different major shells. Therefore, the proton-neutron residual interaction is weaker than proton-proton and neutron-neutron interactions.

One of important sequences of the weak-coupling scheme is that the spectra of even-even nuclei show some similarity and those of odd-even nuclei are clustered around the corresponding parent states. An analysis of the experimental spectra for the nuclei we are concerned with in this paper indeed shows that they display the character of the weak-coupling scheme similar to nuclei with $A\sim 150$ [15] and $A\sim 208$ [14].

The paper is organized as follows: In Sec. II we discuss how the model space and residual interaction are constructed. The calculated results are presented in Sec. III. A discussion and conclusions are given in the last section. All calculations are carried out using the spherical shell model code OXBASH [17].

II. MODEL SPACE AND RESIDUAL INTERACTION

The model space used in this paper is named GWB in the code OXBASH [17]. This model space includes four proton orbitals $(1f_{5/2},2p_{3/2},2p_{1/2},1g_{9/2})$ and six neutron

TABLE I. The maximum dimensions of the m scheme and corresponding projected basis in each nucleus in the truncations of Cal.(II) and Cal.(III).

Nucleus	J^{π}	Cal.(II) m scheme	Cal.(II) Projected basis	Cal.(III) m scheme	Cal.(III) Projected basis
$^{92}_{42}$Mo	6^+	3551	725	342	45
$^{94}_{44}$Ru	6^+	2333	278	294	38
$^{96}_{46}$Pd	6^+	128	39	36	12
$^{94}_{42}$Mo	6^+	4973847	113962	24935	4651
$^{96}_{44}$Ru	6^+	224232	42864	28294	5374
$^{98}_{42}$Pd	6^+	28128	6081	6796	1554
$^{93}_{42}$Mo	$11/2^+$	13967	77655	2883	538
$^{95}_{42}$Mo	$11/2^+$	4359277	636795	8568	1533
$^{95}_{44}$Ru	$11/2^+$	25951	4991	3274	622
$^{95}_{43}$Tc	$11/2^+$	483970	79053	39378	6673

orbitals $(1g_{9/2},2p_{1/2},2d_{5/2},2d_{3/2},3s_{1/2},1g_{7/2})$. The single-particle energies (SPEs) for these orbitals are $\varepsilon_{\pi 1f_{5/2}}=-5.322$ MeV, $\varepsilon_{\pi 2p_{3/2}}=-6.144$ MeV, $\varepsilon_{\pi 2p_{1/2}}=-3.941$ MeV, $\varepsilon_{\pi 1g_{9/2}}=-1.250$ MeV, and $\varepsilon_{\nu 1g_{9/2}}=-2.597$ MeV, $\varepsilon_{\nu 2p_{1/2}}=-0.696$ MeV, $\varepsilon_{\nu 2d_{5/2}}=1.8300$ MeV, $\varepsilon_{\nu 2d_{3/2}}=4.261$MeV, $\varepsilon_{\nu 3s_{1/2}}=1.610$ MeV, and $\varepsilon_{\nu 1g_{7/2}}=5.159$ MeV. The residual interaction corresponding to this model space is also provided in the code named GWBXC, which is a combined effective interaction. First, all the two-body matrix elements (TBMEs) for this model space are generated from the bare G matrix of the H7B potential [19]. Then, the TBMEs for the proton $(1f_{5/2},\ 2p_{3/2},\ 2p_{1/2},\ 1g_{9/2})$ orbitals are replaced by those of Ji and Wildenthal [5]; the proton-neutron TBMEs which connect the $\pi(2p_{1/2},1g_{9/2})$ and $\nu(2d_{5/2},3s_{1/2})$ orbitals are taken from those of Gloeckner [20], and the proton-neutron TBMEs which connect the $\pi(2p_{1/2},1g_{9/2})$ and $\nu(2p_{1/2},1g_{9/2})$ orbitals are taken from those of Serduke *et al.* [6]. Since $N=50$ is a good magic number, we will not take the neutron particle-hole excitations across the $N=50$ shell; i.e., the orbitals $\nu 2p_{1/2}$ and $\nu 1g_{9/2}$ are occupied by two and ten neutrons, respectively. As for the proton valences, we will use three truncation schemes. The shell model code OXBASH [17] follows a hybid algorithm between the m scheme and the jj scheme. The maximum dimensions of the m scheme and the projected basis of each nucleus studied in this paper for Cal.(II) and Cal.(III) [the explanations for Cal.(II) and Cal.(III) are given in detail in the following section] are presented in Table I.

III. CALCULATED RESULTS

A. Binding energies

We first discuss the binding energies of all nuclei in the range $40\leqslant Z\leqslant 50$ and $50\leqslant N\leqslant 52$. These binding energies are essential to determine the beta decay rate in nuclear astrophysics. It also gives a test of the effective interaction and the truncation scheme used in this paper. The results are listed in Table II. The shell model results are those of Cal.(III) (see next subsection for an explanation). The deviations of the experiment [21] and shell model $\Delta=E_b(\text{expt})-E_b(\text{sm})$ are regular. In general, Δ decreases as the neutron and proton numbers increase. This Δ can be divided into the following terms in a general form up to quadratic in the numbers of protons and neutron:

$$\Delta=a+bn_p+cn_p^2+dn_n+en_n^2+fn_pn_n+gn_p^2n_n+hn_pn_n^2+ln_p^2n_n^2, \tag{1}$$

with $n_p=Z-38$ and $n_n=N-50$ representing the valence particles in the orbitals $\pi(g_{9/2},p_{1/2})$ and $\nu(d_{5/2},d_{3/2},s_{1/2},g_{7/2})$. The nine parameters in Eq. (1) were determined in a χ^2 fit to 33Δ. Then their values for the best fit are $a=28.490$ MeV, $b=0.379$ MeV, $c=-0.043$ MeV, $d=-0.223$ MeV, $e=-0.276\times10^{-5}$ MeV, $f=0.028$ MeV, $g=0.510\times10^{-3}$ MeV, $h=-0.259\times10^{-7}$ MeV, and $l=0.503\times10^{-8}$ MeV. The great difference between c and e is relative to the Coulomb energy. There is no Coulomb interaction in the combined interaction GWBXC while the neutron-neutron interaction has been included in the interaction. The parameter f presents a modification of the proton-neutron interaction between the valence protons and neutrons in the model space. As we know, the proton-neutron interaction is more difficult to determine than the like-particle interaction.

We used Eq. (1) to calculate the binding energies for all nuclei in the range $40\leqslant Z\leqslant 50$ and $50\leqslant N\leqslant 52$. A comparison of our fitted energies with the experimental data shows that our truncation scheme is reasonable in most cases. The large δE for nuclei with $Z=40$ and 41 reflects that Cal.(III) cannot reproduce well the results of Cal.(II) for these nuclei.

As we can see the contributions of the nonlinear terms $n_p^2n_n$, $n_pn_n^2$ and $n_p^2n_n^2$ are quite small and can be ignored. Therefore, Eq. (1) is simplified to

$$\Delta'=a+bn_p+cn_p^2+dn_n+en_n^2+fn_pn_n. \tag{2}$$

The binding energies calculated using Eq. (2) are also presented in Table II as $E_b'(\text{fit})$.

Comparisons of the calculated results with the experimental level data [22] for even-even and odd-even nuclei are shown in Figs. 1–12.

B. Structure of the nuclei $^{92}_{42}$Mo$_{50}$, $^{94}_{44}$Ru$_{50}$, $^{96}_{46}$Pd$_{50}$, and $^{92,94}_{40}$Zr$_{52,54}$

The experimental and theoretical low-lying states of $^{92}_{42}$Mo$_{50}$, $^{94}_{44}$Ru$_{50}$ and $^{96}_{46}$Pd$_{50}$ are compared in Figs. 1–3. The low-lying states of these $N=50$ nuclei can be well explained in terms of the proton excitation in the orbitals $1f_{5/2}$,$2p_{3/2}$,$2p_{1/2}$, and $1g_{9/2}$ [2–5]. The points that we calculate with these nuclei are (1) how many partitions are enough to describe the spectra of these nuclei and (2) to show the weak coupling of the proton pairs. It is impossible to diagonalize the Hamiltonian matrix without a restriction on the

TABLE II. The shell model [Cal.(III)] and experimental binding energies (MeV) [with respect to the core $^{66}_{28}$Ni of 33 isotopes with experimental error σ, $\Delta = E_b(\mathrm{expt}) - E_b(\mathrm{sm})$ and $\delta E = E_b(\mathrm{expt}) - E_b(\mathrm{fit})$].

Z	N	Nucleus	E_b(sm)	E_b(expt)	σ	Δ	E_b(fit)	δE	E'_b(fit)
40	50	^{90}Zr	178.404	207.064	0.002	28.640	206.894	−0.170	206.894
	51	^{91}Zr	185.810	214.449	0.002	28.449	214.078	−0.372	214.077
	52	^{92}Zr	194.671	222.894	0.002	28.223	222.716	−0.178	222.716
41	50	^{91}Nb	183.751	212.023	0.003	28.252	212.237	0.213	212.237
	51	^{92}Nb	191.922	220.106	0.003	28.182	220.213	0.107	220.213
	52	^{93}Nb	201.010	228.936	0.002	27.926	229.107	0.171	229.106
42	50	^{92}Mo	191.258	219.679	0.004	28.421	219.654	−0.025	219.654
	51	^{93}Mo	199.562	227.749	0.004	28.187	227.793	0.044	227.791
	52	^{94}Mo	209.421	237.427	0.002	28.006	237.487	0.060	237.483
43	50	^{93}Tc	195.619	223.766	0.004	28.147	223.840	0.074	223.840
	51	^{94}Tc	204.393	232.389	0.004	27.996	232.480	0.091	232.475
	52	^{95}Tc	214.553	242.322	0.005	27.769	242.505	0.183	242.496
44	50	^{94}Ru	202.001	230.013	0.013	28.012	229.963	−0.050	229.963
	51	^{95}Ru	211.037	238.976	0.012	27.969	238.900	−0.080	238.888
	52	^{96}Ru	221.876	249.660	0.008	27.784	249.632	−0.028	249.615
45	50	^{95}Rh	205.456	233.070	0.150	27.614	233.073	0.003	233.073
	51	^{96}Rh	215.109	242.430	0.013	27.322	242.656	0.226	242.643
	52	^{97}Rh	226.022	253.470	0.040	27.448	253.498	0.028	253.472
46	50	^{96}Pd	210.865	238.200	0.150	27.335	238.053	−0.147	238.053
	51	^{97}Pd	220.572	247.890	0.300	27.318	247.722	−0.168	247.704
	52	^{98}Pd	232.136	259.460	0.022	27.324	259.249	−0.211	259.212
47	50	^{97}Ag	213.420	240.110	0.400	26.690	240.093	−0.017	240.093
	51	^{98}Ag	223.718	250.260	0.150	26.542	250.388	0.128	250.363
	52	^{99}Ag	235.373	262.180	0.150	26.807	262.041	−0.139	261.991
48	50	^{98}Cd	217.887	244.060	0.210	26.173	243.961	−0.099	243.961
	51	^{99}Cd	228.402	254.530	0.210	26.402	254.508	−0.022	254.476
	52	^{100}Cd	240.549	266.554	0.110	26.005	266.688	0.134	266.623
49	50	^{99}In	219.543	244.810	0.500	25.267	244.932	0.122	244.932
	51	^{100}In	230.732	255.700	0.400	24.968	256.190	0.490	256.149
	52	^{101}In	242.953	268.450	0.300	25.497	268.481	0.031	268.398
50	50	^{100}Sn	223.084	247.650	0.450	24.566	247.704	0.054	247.704
	51	^{101}Sn	233.782	258.820	0.500	25.038	258.509	−0.312	258.458
	52	^{102}Sn	247.332	272.082	0.400	24.748	272.165	0.083	272.063

filling of the valence protons in the selected model space and a suitable truncation must be proposed. In order to do so, first, we used ^{88}Sr as an inert core; i.e., only the $Z-38$ valence protons are active in $1g_{9/2}$ and $2p_{1/2}$ orbitals and the results are shown in Figs. 1(a), 2(a), and 3(a) [referred to as Cal.(I)]. As noted from the figures, the calculated results are not in agreement with the corresponding experimental data. Therefore, more configurations should be taken into account to improve the calculation. Second, at most up to two protons are allowed to excite from the orbitals $\pi 1f_{5/2}$ and/or $\pi 2p_{3/2}$ across the ^{88}Sr core into the orbitals $\pi 2p_{1/2}$ and $\pi 1g_{9/2}$ and the calculated levels are shown in Figs. 1(b), 2(b), and 3(b) by solid lines [referred to as Cal.(II)]. As can be seen, the agreement with the experimental spectra is quite good. But as we will show later, such a configuration space is too large when combined with the neutron configurations in $(2d_{5/2}, 2d_{3/2}, 3s_{1/2}, 1g_{7/2})$ model space to calculate nuclei with $N > 50$. We should pick up configurations that can reproduce the results of Cal.(II). This can be done by selecting the dominate partitions of Cal.(II). In the calculation, we find out that the results of Cal.(II) can be well reproduced when we select partitions with weight $P \geqslant 2\%$ in the wave functions of Cal.(II) to diagonalize the Hamiltonian [referred to as Cal.(III)]. The results are shown by the dashed line in Figs. 1(b), 2(b), and 3(b). We note that, on the one hand, Cal.(III) can reproduce well the results of Cal.(II) except for a few states. For example, the second 0^+ state in Cal.(II) in $^{94}_{44}$Ru$_{50}$ agrees with the experimental excitation energy and the weights of the partitions $\pi p^2_{1/2} g^4_{9/2}$ and $\pi g^6_{9/2}$ are 24% and 46%. The rest of the partitions are dominated by $\pi f^{-2}_{5/2} p^2_{1/2} g^6_{9/2}$ with 20%, while in Cal.(III), the wave function is dominated by the partition $\pi g^6_{9/2}$ (80%). The rest of the states shown in Figs. 1(b), 2(b), and 3(b) of the two calculations all have a small difference in the binding energies, excited energies, and wave function structure. In Table III, the binding energies (with respect to the core $^{66}_{28}$Ni), the excited energies, and the wave functions of the lowest 0^+–8^+ states for

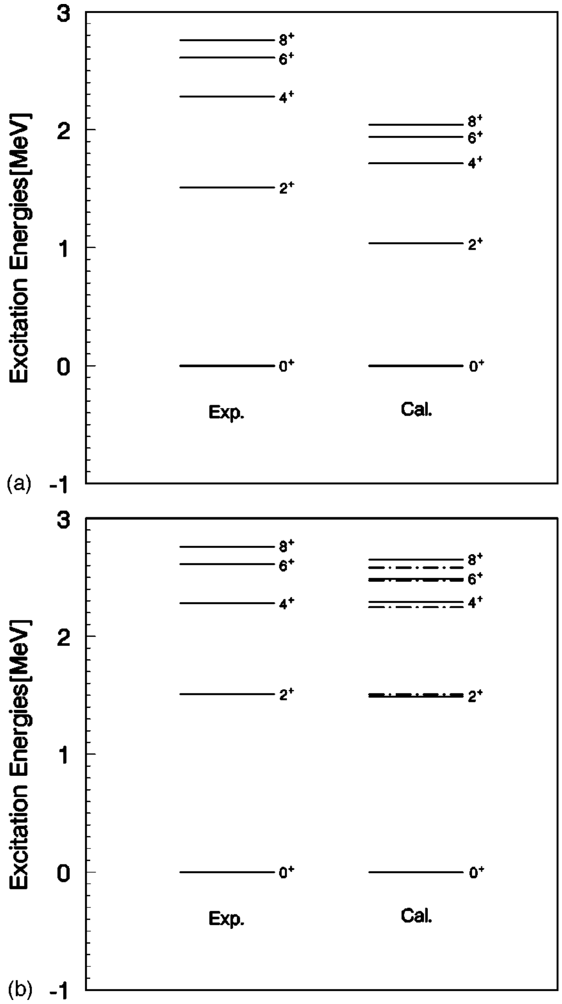

FIG. 1. (a) Comparison of the experimental and theoretical energy levels of ${}^{92}_{42}\mathrm{Mo}_{50}$. The calculated result takes ${}^{88}\mathrm{Sr}$ as an inert core [referred to as Cal.(I)]. (b) Comparison of the experimental and theoretical energy levels of ${}^{92}_{42}\mathrm{Mo}_{50}$. The solid lines are the results of Cal.(II) in which, at most, up to two protons can be excited from $1f_{5/2}$ and/or $2p_{3/2}$ orbitals up to the ${}^{88}\mathrm{Sr}$ core. The dashed lines are the results of selecting configurations with $P \geqslant 2\%$ of Cal.(II) and referred to as Cal.(III).

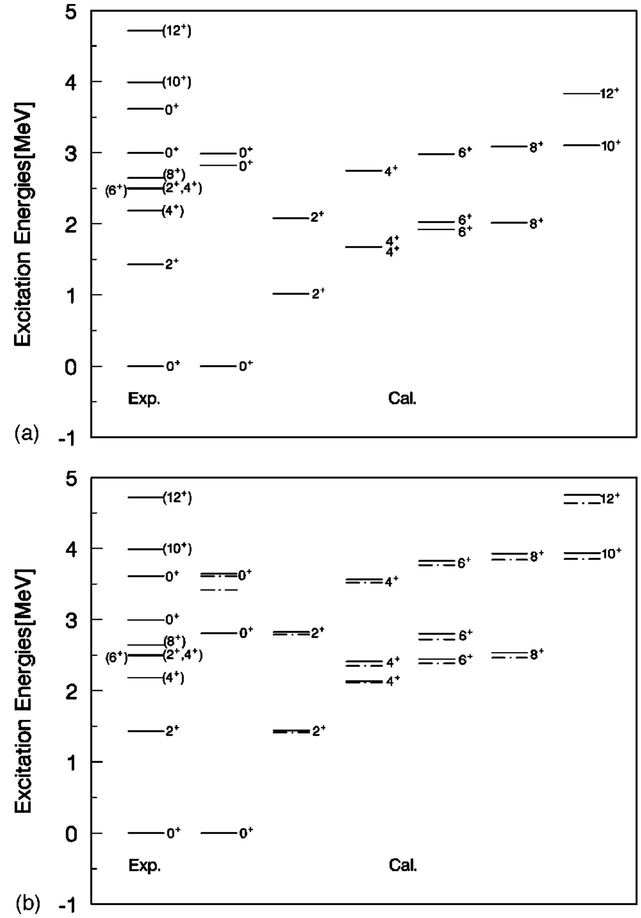

FIG. 2. (a) Comparision of the experimental and theoretical energy levels of ${}^{94}_{44}\mathrm{Ru}_{50}$. The evaluated data are the result of Cal.(I). (b) Comparison of the experimental and theoretical energy levels of ${}^{94}_{44}\mathrm{Ru}_{50}$. The solid lines are the results of Cal.(II) and the dashed lines the results of Cal.(III).

${}^{92}_{42}\mathrm{Mo}$, ${}^{94}_{44}\mathrm{Ru}$, and ${}^{96}\mathrm{Pd}$ are listed. The evaluated $8^+ \rightarrow 6^+ \rightarrow 4^+ \rightarrow 2^+ \rightarrow 0^+$ $E2$ transition rates for ${}^{92}_{42}\mathrm{Mo}$ in the cases of Cal.(II) and Cal.(III) also have a small difference (see Table IV). Therefore, it may be reasonable to use the proton partitions of Cal.(III) to calculate nuclei with $N>50$. On the other hand, the dimension of the Hamiltonian matrix is greatly reduced in Cal.(III). For instance, the dimension of the matrix for 6^+ in ${}^{92}_{42}\mathrm{Mo}$ in Cal.(II) is 725, while it is 45 in Ca.(III) (see Table I). We should also point out it is very difficult, even impossible, to perform the calculation for nuclei with $N>50$ using the partitions of Cal.(II) with the code OXBASH due to the huge dimension of the Hamiltonian matrix. For example, the maximum projected dimension in ${}^{94}_{42}\mathrm{Mo}$ is 113 962 using the proton partitions of Cal.(II) of ${}^{92}_{42}\mathrm{Mo}$, which is very difficult to handle, while it is 4651 when using the partitions of Cal.(III), which is much smaller and manageable. Because of the above two reasons, in the following calculations for nuclei with $N>50$, if not mentioned, the corresponding proton partitions of Cal.(III) with $N=50$ nuclei are used, combining all possible neutron partitions in $d_{5/2}, d_{3/2}, s_{1/2}$, and $g_{7/2}$ orbitals. For example, when we calculate the spectrum of ${}^{94}_{42}\mathrm{Mo}$, we utilize the proton partitions of Cal.(III) of the nucleus ${}^{92}_{42}\mathrm{Mo}$ and combine all possible two-neutron partitions in model space ($d_{5/2}, d_{3/2}, s_{1/2}$, and $g_{7/2}$). If possible, we also carry out calculations utilizing the proton partitions of Cal.(II) for comparison.

The spectra of the nuclei ${}^{92}_{42}\mathrm{Mo}_{50}$, ${}^{94}_{44}\mathrm{Ru}_{50}$, and ${}^{96}_{46}\mathrm{Pd}_{50}$ (Figs. 1–3) indicate the weak coupling between the proton pairs in Cal.(I), (II), and (III), even though the results of Cal.(I) are not in good agreement with the experimental data. This is because the shell model Hamiltonians, as we mentioned in Sec. I and displayed in Refs. [14–16], have the weak-coupling feature for midheavy and heavy nuclei. The spectrum of ${}^{96}_{46}\mathrm{Pd}_{50}$ can be explained in terms of the weak coupling between two proton-hole pairs and, therefore, is almost the same as that of ${}^{94}_{44}\mathrm{Ru}_{50}$.

The three low-lying states of ${}^{92,94}_{40}\mathrm{Zr}_{52,54}$ shown in Fig. 4 can be well explained as the excitations of one neutron pair

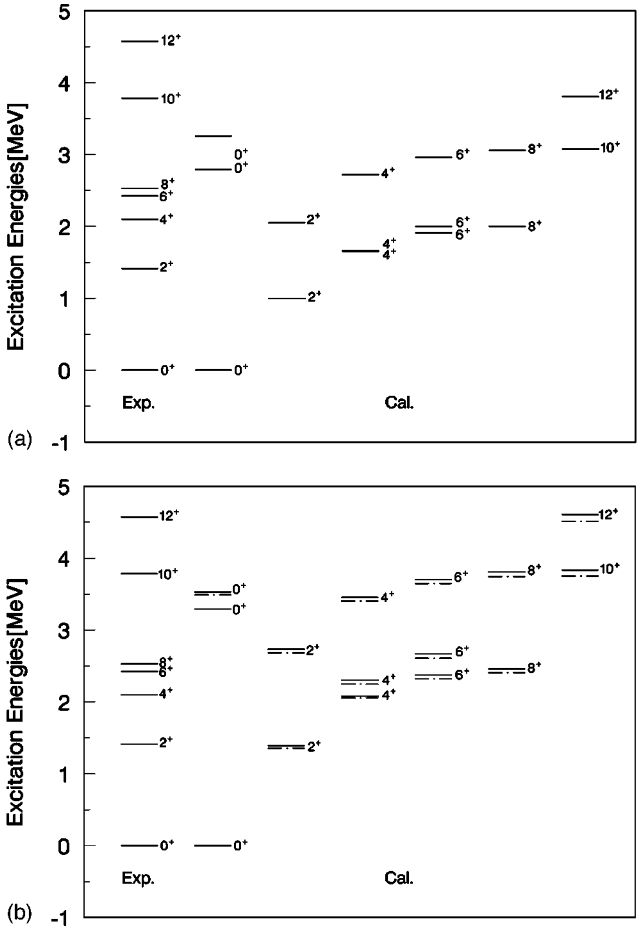

FIG. 3. (a) The same as in Fig. 2(a) but for the nucleus ${}^{96}_{46}Pd_{50}$. (b) The same as in Fig. 2(b) but for the nucleus ${}^{96}_{46}Pd_{50}$.

and one neutron-hole pair in a $2d_{5/2}$ orbital, respectively (see also the wave functions listed in Table III).

The neutron pair in the nucleus ${}^{92}_{40}Zr_{52}$ and proton pair in the nucleus ${}^{92}_{42}Mo_{50}$ provide the basic building blocks to establish the low-lying spectra of other nuclei discussed in the following. This is quite similar to the cases in the $A\sim150$

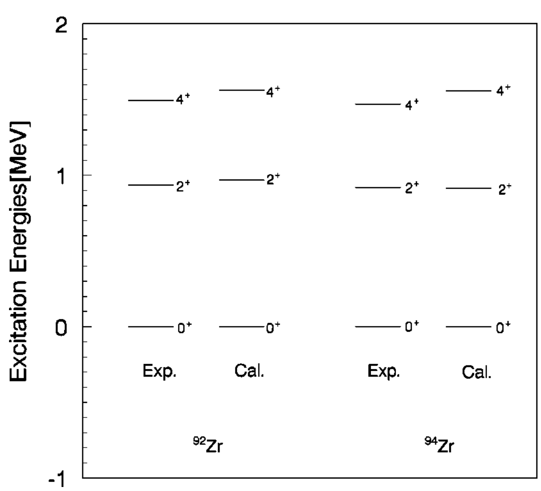

FIG. 4. The experimental and calculated energy levels of ${}^{92,94}_{40}Zr_{52,54}$.

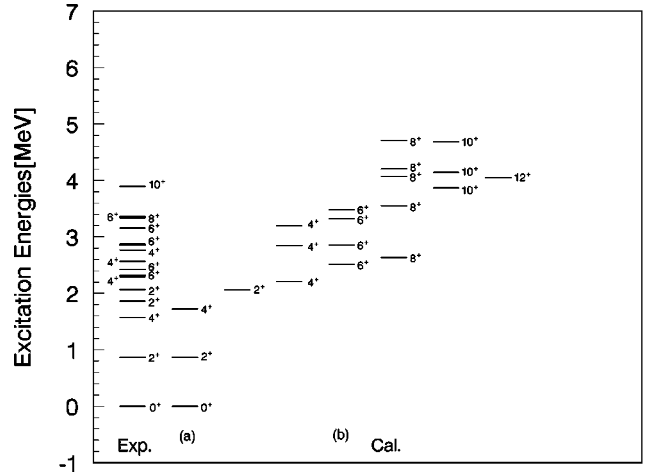

FIG. 5. The experimental and theoretical energy levels of ${}^{94}_{42}Mo_{52}$ for the positive parity states.

mass region [15]. The spectra of the even-even nuclei ${}^{94}_{40}Zr_{54}$, ${}^{94}_{42}Mo_{52}$, ${}^{94,96}_{44}Ru_{50,52}$, and ${}^{96,98}_{46}Pd_{50,52}$ can be well described by the weak coupling of proton pairs, and neutron pairs, and the spectra of the odd-even nuclei ${}^{93,95}_{42}Mo_{51,53}$, ${}^{95}_{43}Tc_{52}$, and ${}^{95}_{44}Ru_{51}$ are clustered around the corresponding parent states by weakly coupling the odd nucleon to parent states of the even-even nuclei.

C. Structure of the nuclei ${}^{94}_{42}Mo_{52}$, ${}^{96}_{44}Ru_{52}$, and ${}^{98}_{46}Pd_{52}$

Comparisons of the experimental and calculated levels are shown in Figs. 5–7. In these figures, the experimental states with determined spins and parities are presented. We believe that our calculation can help experiments to determine the spins and parities of those undetermined states. The calculated results are in good agreement with the experimental data. This shows the validity of our truncation scheme. A similar structure is clearly displayed among the spectra of these nuclei in both experimental and theoretical data. The three low-lying states $[0^+,2^+,4^+$ states of set (a)] of these nuclei have similar excitation energies and wave function structures; i.e., they are approximately equal to those of

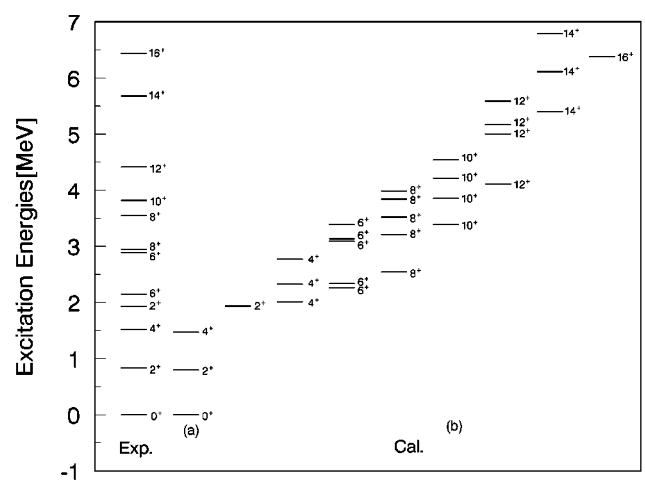

FIG. 6. The experimental and theoretical energy levels of ${}^{96}_{44}Ru_{52}$ for the positive parity states.

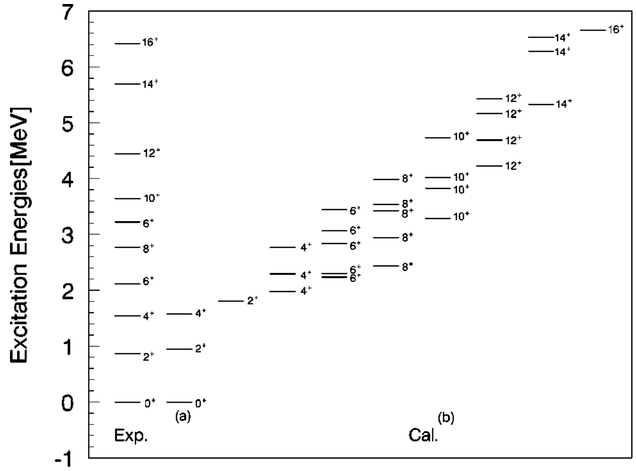

FIG. 7. The experimental and theoretical energy levels of ${}^{98}_{46}\mathrm{Pd}_{52}$ for the positive parity states.

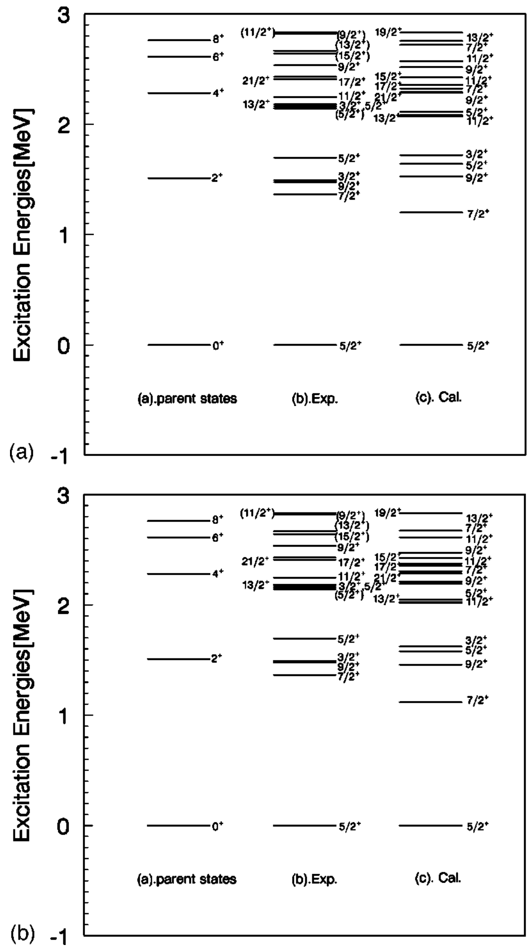

FIG. 8. (a) The parent states and experimental and calculated states [Cal.(III)] of ${}^{93}_{42}\mathrm{Mo}_{51}$ for the positive parity states. (b) The parent states and experimental and calculated states of ${}^{93}_{42}\mathrm{Mo}_{51}$ for the positive parity states using the valence proton partitions of Cal.(II).

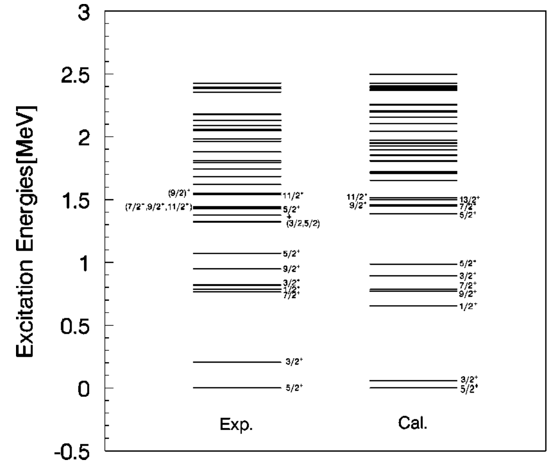

FIG. 9. The experimental and calculated states of ${}^{95}_{42}\mathrm{Mo}_{53}$ for the positive parity states.

${}^{92,94}_{40}\mathrm{Zr}_{52,54}$ which mainly arise from the excitation of the neutron pair. The main configurations of these states are listed in Table V. The calculated $B(E2)$'s for $4^+ \rightarrow 2^+ \rightarrow 0^+$ transitions are presented in Table VI. Both strengths contributed by the neutrons and the total of $B(E2)$'s in these nuclei are similar. These similar $B(E2)$ strengths support the above similar wave function structure. Measuring these $B(E2)$'s will directly test the weak-coupling picture in these excited states. The lowest states 2^+, 4^+, 6^+, and 8^+ of set (b) in Figs. 5–7 can be explained as the proton pair excited states, and their excited energies are approximately equal to those of the low-lying states of ${}^{92}_{42}\mathrm{Mo}_{50}$. The other states result from the coupling between proton pairs and neutron pairs. The similarity of the spectra of the nuclei ${}^{94}_{42}\mathrm{Mo}_{52}$, ${}^{96}_{44}\mathrm{Ru}_{52}$, and ${}^{98}_{46}\mathrm{Pd}_{52}$ clearly indicates the weak coupling of the proton pairs and neutron pairs and is similar to the similarity between the spectra of ${}^{150}_{66}\mathrm{Dy}$ and ${}^{152}_{68}\mathrm{Er}$ shown in Ref. [15]. Therefore, the concepts proposed and conclusions drawn in Ref. [15] about the independent nucleon-pair motion are all applicable to the nuclei discussed here. The goodness of the

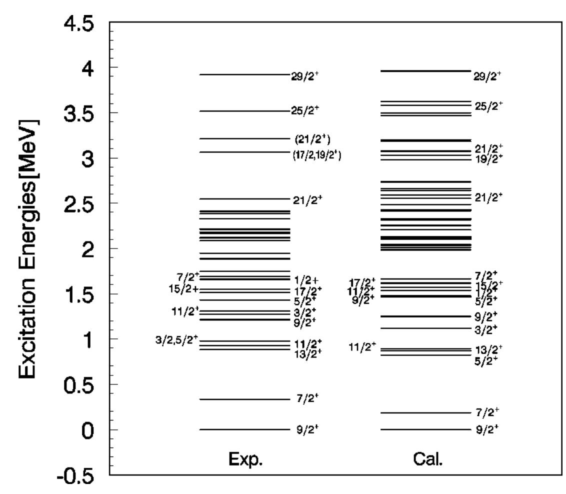

FIG. 10. The experimental and calculated states of ${}^{95}_{43}\mathrm{Tc}_{52}$ for the positive parity states.

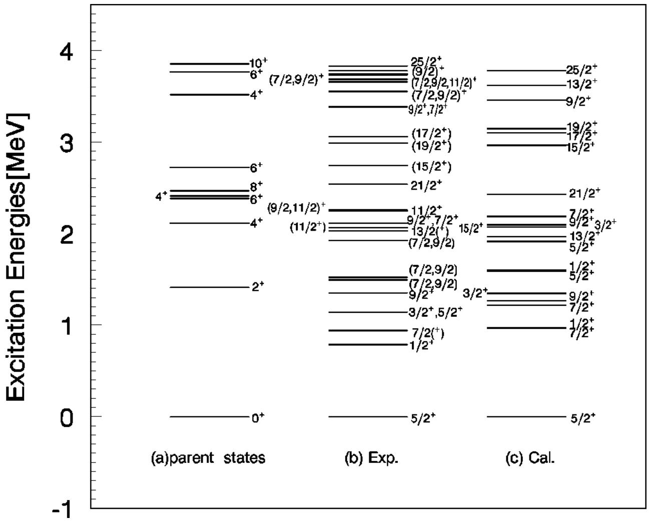

FIG. 11. The parent states and experimental and calculated states of ${}^{95}_{44}\mathrm{Ru}_{51}$ for the positive parity states.

similarity among the spectra of ${}^{94}_{42}\mathrm{Mo}_{52}$, ${}^{96}_{44}\mathrm{Ru}_{52}$, and ${}^{98}_{46}\mathrm{Pd}_{52}$ is, however, a little poorer than that between the spectra of ${}^{150}_{66}\mathrm{Dy}$ and ${}^{152}_{68}\mathrm{Er}$. This is due to the following facts: (1) the residual interaction here is stronger than that for the nuclei in the $A\sim150$ mass region if one considers the expirical relation $V=A^{-1/3}$ between the TBME V and the mass A; (2) the configuration mixings are more complicated because of the stronger residual interaction and the easy break of the $Z=40$, even the $Z=38$ subshell; (3) the spectra of ${}^{150}_{66}\mathrm{Dy}$ and ${}^{152}_{68}\mathrm{Er}$ can be well described by one configuration $\pi(s_{1/2}d_{3/2}h_{11/2})^z\nu f^n_{7/2}$ because of the large gap between $\nu f_{7/2}$ and other neutron single-particle energies, while such a gap here between $\nu d_{5/2}$ and other neutron orbitals does not exist. The actual SPEs for $\nu s_{1/2}$, $\nu g_{7/2}$, and $\nu d_{3/2}$ are about 0.6, 0.9, and 1.5 MeV above that of $\nu d_{5/2}$. The structures of the spectra are a result of the weak coupling between many configurations and, therefore, are more complicated and less regular here. This is especially true for the odd-even nuclei discussed in the following.

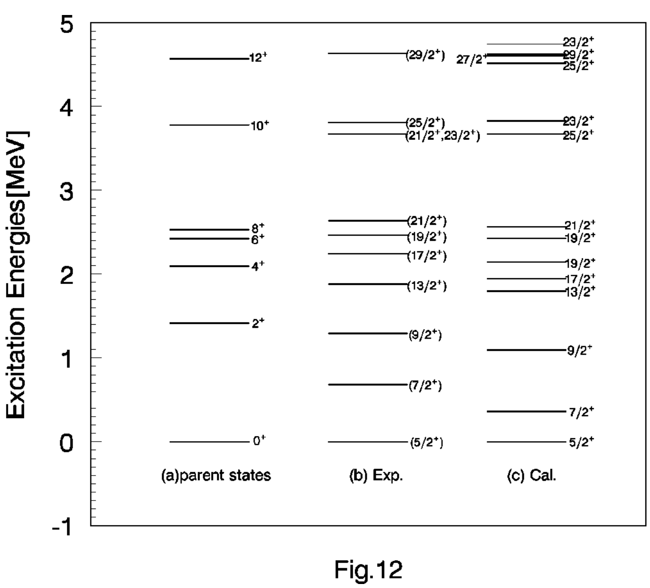

FIG. 12. The parent states and experimental and calculated states of ${}^{97}_{46}\mathrm{Pd}_{51}$ for the positive parity states.

TABLE III. (a) Comparisons of the binding energies, the excitation energies, the main configurations (Conf.) (πg^2) of the 0^+-8^+ states in ${}^{92}_{42}\mathrm{Mo}_{50}$ calculated using the proton partitions of Cal.(II) and Cal.(III). (b) Comparisons of the binding energy, the excitation energies, the main configurations (Conf.) (πg^4) of the lowest $0^+–8^+$ states in ${}^{94}_{44}\mathrm{Ru}_{50}$ calculated using the proton partitions of Cal.(II) and Cal.(III). (c) Comparisons of the binding energy, the excitation energies, the main configurations (Conf.) (πg^6) of the lowest $0^+–8^+$ states in ${}^{96}_{46}\mathrm{Pd}_{50}$ calculated using the proton partitions of Cal.(II) and Cal.(III).

		(a)			
J^π	0^+	2^+	4^+	6^+	8^+
E (MeV) (II)	191.621	1.470	2.291	2.490	2.653
Conf.	56.25	65.16	69.22	69.04	70.38
E (MeV) (III)	191.258	1.507	2.249	2.475	2.582
Conf.	70.48	80.70	80.82	81.47	80.91
E (MeV) (Expt.)	219.679	1.509	2.282	2.612	2.760
		(b)			
E (MeV) (II)	202.233	1.441	2.136	2.447	2.535
Conf.	67.25	77.00	76.90	79.60	78.57
E (MeV) (III)	202.001	1.413	2.116	2.384	2.466
Conf.	76.75	85.04	85.31	85.42	85.37
E (MeV) (Expt.)	230.013	1.431	2.186	2.498	2.644
		(c)			
E (MeV) (II)	210.984	1.345	2.034	2.328	2.414
Conf.	81.26	88.91	88.92	89.54	89.42
E (MeV) (III)	210.685	1.356	2.057	2.321	2.405
Conf.	83.68	91.56	91.96	91.99	91.99
E (MeV) (Expt.)	238.200	1.415	2.099	2.424	2.530

D. Structure of the nuclei ${}^{93,95}_{42}\mathrm{Mo}_{51,53}$, ${}^{95}_{43}\mathrm{Tc}_{52}$, ${}^{95}_{44}\mathrm{Ru}_{52}$, and ${}^{97}_{46}\mathrm{Pd}_{51}$

Comparisons of experimental data and the calculated results for these odd-even nuclei are shown in Figs. 8–12. As seen from these figures, the agreement of the theoretical and experimental data is very good. The cluster structure of the spectra of these nuclei around the corresponding even-even parent nuclei is clearly displayed and shows a homologous structure. To further verify, we calculate the one-particle shell model spectroscopic factor $S^{1/2}(J;J_c,j)$ which is defined as

TABLE IV. Comparisons of the $B(E2\text{'s})(e^2\,\mathrm{fm}^4)$ of the Cal.(II) and Cal.(III), and experimental results for the nucleus ${}^{92}_{42}\mathrm{Mo}$. $e^p_{\mathrm{eff}}=1.5e$ is used in the calculation. The experimental data were taken from Ref. [23].

Transition	$B(E2)$(Cal.(II))	$B(E2)$(Cal.(III))	$B(E2)$(Expt.)
$2^+\to0^+$	150.40	122.80	214.31
$4^+\to2^+$	78.50	106.90	-
$6^+\to4^+$	63.40	72.23	82.23
$8^+\to6^+$	25.47	28.56	32.64

TABLE V. The excitation energies, the main configurations of the lowest-lying states 0^+, 2^+, and $4^+(P\%)$ in the nuclei ${}^{92}_{40}\mathrm{Zr}_{52}$, ${}^{94}_{40}\mathrm{Zr}_{54}$, ${}^{94}_{42}\mathrm{Mo}_{52}$, ${}^{96}_{44}\mathrm{Ru}_{52}$, and ${}^{96}_{46}\mathrm{Pd}_{52}$. The configurations listed for ${}^{92}_{40}\mathrm{Zr}_{52}$ and ${}^{94}_{40}\mathrm{Zr}_{54}$ are $\nu d^2_{5/2}$ and $\nu d^4_{5/2}$, respectively, and for ${}^{94}_{42}\mathrm{Mo}_{52}$, ${}^{96}_{44}\mathrm{Ru}_{52}$, and ${}^{98}_{46}\mathrm{Pd}_{52}$ are $\pi g^2_{9/2}\nu d^2_{5/2}$, $\pi g^4_{9/2}\nu d^2_{5/2}$, and $\pi g^6_{9/2}\nu d^2_{5/2}$, respectively.

	J^π	0^+	2^+	4^+
${}^{92}_{40}\mathrm{Zr}_{52}$	Conf.	67.20	73.30	77.15
	$E_{\mathrm{calc.}}$ (MeV)	0.000	0.969	1.562
	$E_{\mathrm{expt.}}$ (MeV)	0.000	0.934	1.495
${}^{94}_{40}\mathrm{Zr}_{54}$	Conf.	72.19	75.71	80.24
	$E_{\mathrm{calc.}}$ (MeV)	0.000	0.913	1.558
	$E_{\mathrm{expt.}}$ (MeV)	0.000	0.919	1.470
${}^{94}_{42}\mathrm{Mo}_{52}$	Conf.	72.28	78.28	75.94
	$E_{\mathrm{calc.}}$ (MeV)	0.000	0.867	1.722
	$E_{\mathrm{expt.}}$ (MeV)	0.000	0.871	1.574
${}^{96}_{44}\mathrm{Ru}_{52}$	Conf.	68.68	74.02	71.95
	$E_{\mathrm{calc.}}$ (MeV)	0.000	0.895	1.605
	$E_{\mathrm{expt.}}$ (MeV)	0.000	0.833	1.518
${}^{98}_{46}\mathrm{Pd}_{52}$	Conf.	68.52	74.06	77.22
	$E_{\mathrm{calc.}}$ (MeV)	0.000	0.919	1.570
	$E_{\mathrm{expt.}}$ (MeV)	0.000	0.863	1.541

$$S^{1/2}(J;J_c,j)=|\langle J||a_j^\dagger||J_c\rangle|/\sqrt{2J+1}, \tag{3}$$

where $|J\rangle$, $|J_c\rangle$, and j are the homologus state, the parent state, and the last odd nucleon single-particle state. This $S^{1/2}(J;J_c,j)$ can provide a sensitive test of the weak coupling between the parent and the last odd nucleon. If the interaction of the parent state and the last odd nucleon vanishes and there is only one j, we should have $S^{1/2}=1$. We present here the results, as examples, of those states in ${}^{93}_{42}\mathrm{Mo}$, i.e., $J=J_c+\nu d_{5/2}$ with $J_c=0^+$, 2^+, 4^+, 6^+, and 8^+ in ${}^{92}_{42}\mathrm{Mo}$: $S^{1/2}(5/2^+;0,\nu d_{5/2})=0.906$, $S^{1/2}(9/2^+;2,\nu d_{5/2})=0.819$, $S^{1/2}(13/2^+;4,\nu d_{5/2})=0.717$, $S^{1/2}(17/2^+;6,\nu d_{5/2})=0.935$, and $S^{1/2}(21/2^+;8,\nu d_{5/2})=0.994$, which show that these states can be well described by weak coupling a $\nu d_{5/2}$ to the parent states of ${}^{92}_{42}\mathrm{Mo}$. Similar results are obtained for other states and other nuclei. Therefore, the explanation proposed in Refs. [14–16] is also applicable to the structures of the spectra of these odd-even nuclei; i.e., the levels of ${}^{93}_{42}\mathrm{Mo}_{51}$, ${}^{95}_{42}\mathrm{Mo}_{53}$, ${}^{95}_{43}\mathrm{Tc}_{52}$, ${}^{95}_{44}\mathrm{Ru}_{51}$, and ${}^{97}_{46}\mathrm{Pd}_{51}$ arise from weak coupling the odd proton or neutron to the corresponding parent states in ${}^{92}_{42}\mathrm{Mo}_{50}$, ${}^{94}_{42}\mathrm{Mo}_{52}$, and ${}^{94}_{44}\mathrm{Ru}_{50}$, respectively. This is especially true for high-spin states. For example, the high-spin states $23/2^+-29/2^+$ and $21/2^+-25/2^+$ in ${}^{97}_{46}\mathrm{Pd}_{51}$ can be well explained as a $\nu d_{5/2}$ weak coupling to the parent state 12^+ and 10^+ in ${}^{96}_{46}\mathrm{Pd}_{50}$, respectively. The ${}^{93}_{42}\mathrm{Mo}_{51}$, ${}^{95}_{44}\mathrm{Ru}_{51}$, and ${}^{97}_{46}\mathrm{Pd}_{51}$ can also be calculated using the proton partitions of Cal.(II). In Fig. 8(b), we show the calculated results for the spectrum of ${}^{93}_{42}\mathrm{Mo}_{51}$ using the proton partitions of Cal.(II). As can be seen, this calculated spectrum is quite similar to that of Cal.(III) [Fig. 8(a)]. The corresponding wave functions whose parent state is 2^+ are listed in Table VII. We can see that the two calculated wave functions have small differences (about 6%). Similar results are obtained for ${}^{95}_{44}\mathrm{Ru}_{51}$ and ${}^{97}_{46}\mathrm{Pd}_{51}$ but one should add some restrictions on the occupation of the valence neutrons in these cases. Therefore, the truncation method we used is reasonable for most of the low-lying states we discuss in this paper. Again, the goodness of the cluster structure, especially for the high-lying states, is poorer than that in the $A\sim150$ mass region for the same reasons discussed in the above subsection. For neutron odd-even nuclei, the coupling between the odd neutron in $s_{1/2}$, $d_{3/2}$ and the parent states $(\phi^{\mathrm{parent}}_{J\alpha}\otimes\phi^n_{s_{1/2},d_{3/2}})$ is also very weak, but these configurations will make the cluster structure less regular when they mix with the configuration $\phi^{\mathrm{parent}}_{J\alpha}\otimes\phi^n_{d_{5/2}}$. As for the configuration $\phi^{\mathrm{parent}}_{J\alpha}\otimes\nu g_{7/2}$, its coupling is much stronger, especially when the valence protons or neutrons increase. There are many other states that can be explained as a weak coupling of the last odd nucleon to the parent states which are dominated configurations by exciting more protons up the $Z=38$ subshell, even by breaking the $N=50$ major shell. The calculation for these states is more difficult and unstable because the main parts of the interaction GWBXC are determined with $Z=38$ as a subshell.

It is interesting to note that the low-lying states of ${}^{95}_{42}\mathrm{Mo}_{53}$

TABLE VI. The calculated and experimental $B(E2)$'s (e^2 fm^4) for the nuclei ${}^{92}_{40}\mathrm{Zr}$, ${}^{94}_{40}\mathrm{Zr}{}^{94}_{42}\mathrm{Mo}$, ${}^{96}_{44}\mathrm{Ru}$, and ${}^{98}_{46}\mathrm{Pd}$. The $e^p_{\mathrm{eff}}=1.5e$ and $e^n_{\mathrm{eff}}=0.5e$ are used in the calculation. The experimental data were taken from Refs. [24,25].

${}^{92}_{40}\mathrm{Zr}$	$B(E2)$ (neutron)	$B(E2)$ (total)	$B(E2)$ (Expt.)
$2^+\to0^+$	11.59	100.6	-
$4^+\to0^+$	15.77	154.4	-
${}^{94}_{40}\mathrm{Zr}$	$B(E2)$ (neutron)	$B(E2)$ (total)	$B(E2)$ (Expt.)
$2^+\to0^+$	10.20	94.9	-
$4^+\to0^+$	18.37	171.4	-
${}^{94}_{42}\mathrm{Mo}$	$B(E2)$ (neutron)	$B(E2)$ (total)	$B(E2)$ (Expt.)
$2^+\to0^+$	9.91	158.5	395.40 [24]
$4^+\to0^+$	10.38	166.1	666.74 [24]
${}^{96}_{44}\mathrm{Ru}$	$B(E2)$ (neutron)	$B(E2)$ (total)	$B(E2)$ (Expt.)
$2^+\to0^+$	13.00	239.0	476.32 [25]
$4^+\to0^+$	13.45	213.1	553.85 [25]
${}^{98}_{46}\mathrm{Pd}$	$B(E2)$ (neutron)	$B(E2)$ (total)	$B(E2)$ (Expt.)
$2^+\to0^+$	13.72	248.8	-
$4^+\to0^+$	15.17	219.0	-

TABLE VII. Comparisons of the excitation energies, the main configurations (Conf.) of the states in ${}^{93}_{42}\mathrm{Mo}_{51}$ whose parent state is 2^+ calculated using the proton partitions of Cal.(II) and Cal.(III). The main configuration of states $3/2^+$–$9/2^+$ is $(\pi g^2_{9/2})_2\otimes\nu d^1_{5/2}$ and of state $1/2^+$ is $(\pi g^2_{9/2})_0\otimes\nu s^1_{1/2}$.

J^π	$9/2^+$	$7/2^+$	$5/2^+$	$3/2^+$	$1/2^+$
E (MeV) (II)	1.458	1.118	1.580	1.623	1.355
Conf.	78.14	76.86	73.63	60.33	42.00
E (MeV) (III)	1.532	1.199	1.653	1.716	1.357
Conf.	83.32	82.14	79.28	66.62	49.19

(Fig. 9) and $^{95}_{43}\mathrm{Tc}_{52}$ (Fig. 10) show a similar structure. These two nuclei have the same parent nuclei, i.e., $^{94}_{42}\mathrm{Mo}_{52}$. The low-lying states up to 2.5 MeV of $^{95}_{42}\mathrm{Mo}_{53}$ can be obtained by simply replacing the last odd proton in $^{95}_{43}\mathrm{Tc}_{52}$ with a neutron and vice versa, particularly to the states which arise from coupling the last odd nucleon to the low-lying 0^+, 2^+, and 4^+ parent states. We label all the spins and parities states whose parent states are those of set (a) in Fig. 5. If the single-particle angular momentum of the last odd nucleon is the same, the states of the two nuclei, which share the same parent state, can correspond each to other one to one. Such a structure also appears in the high-lying states in nuclei $^{206}_{82}\mathrm{Pb}$ and $^{206}_{81}\mathrm{Tl}$, which can be well described by weakly coupling a $\pi h_{9/2}$ and a $\nu g_{9/2}$ to the low-lying states of $^{205}_{81}\mathrm{Tl}$. In this case, the parities of the $\pi h_{9/2}$ and $\nu g_{9/2}$ are opposite. We will present the results of this special structure between $^{206}_{82}\mathrm{Pb}$ and $^{206}_{81}\mathrm{Tl}$ elsewhere [26].

In all, as far as the nuclei we are concerned with here, the weak-coupling scheme works quite well. This weak-coupling scheme, as mentioned above, is rooted in the shell model Hamiltonian and should not be changed if one extends or restricts the configuration space. As we have shown, both the results of Cal.(II) and Cal.(III) show the weak coupling between proton pairs in $^{94}_{44}\mathrm{Ru}$ and $^{96}_{46}\mathrm{Pd}$ and between the odd neutron and the even-even parent states in $^{93}_{42}\mathrm{Mo}$, etc. The results of Cal.(I) also show the same weak-coupling structure between proton pairs in $^{94}_{44}\mathrm{Ru}$ and $^{96}_{46}\mathrm{Pd}$, but the configuration space of Cal.(I) is too small to give a reasonable description of the spectra for nuclei with $N=50$ and, therefore, is not used to calculate those nuclei with $N>50$.

We should point out that the weak-coupling scheme provides a reasonable explanation why our truncation of Cal.(III) is effective for nuclei with $N>50$. The reason is given as follows. In the weak-coupling model [18], the Hamiltonian can be separated into three parts:

$$H=H_1+H_2+V_{12}. \tag{4}$$

The H_1 and H_2 parts of the Hamiltonian are diagonalized separately:

$$\begin{aligned} H_1\phi^1_{J_1\alpha}&=E^1_{J_1\alpha}\phi^1_{J_1\alpha}, \\ H_2\phi^2_{J_2\beta}&=E^2_{J_2\beta}\phi^2_{J_2\beta}, \end{aligned} \tag{5}$$

where $J_1\alpha$ and $J_2\beta$ are two complete sets of quantum numbers needed to label the corresponding eigenstates. The total H of Eq. (4) can be diagonalized in the bases

$$\Psi_{J\nu}=[\phi^1_{J_1\alpha}\otimes\phi^2_{J_2\beta}]_{J\nu}. \tag{6}$$

In general, in order to get an equal result to that obtained by directly diagonalizing the whole H, one should include all possible bases $\Psi_{J\nu}$ to diagonalize the whole Hamiltonian. If V_{12} is small, it will not change the wave function structures of H_1 and H_2 when diagonalizing the total H. Therefore, we can select the dominate wave functions $\phi_{J_1\alpha}$ and $\phi_{J_2\beta}$, which can well reproduce the spectra of H_1 and H_2. That means that because of the weak coupling between H_1 and H_2, the combined configurations $\Psi_{J\nu}$ are also energetically favored for the whole H if the corresponding $\phi^1_{J_1\alpha}$ and $\phi^2_{J_2\alpha}$ are energetically favored for H_1 and H_2, respectively. In this way, we can reduce the dimension of the total Hamiltonian matrix without losing much accuracy. Since the valence neutron number is small in our calculation (we take $N=50$ as the neutron core for all nuclei), we include all neutron partitions. We should mention that our way selecting the configurations shares some similarity to that of Horoi *et al.* [13]. Both ways pick up the energetically favored configurations to reduce the dimension of the Hamiltonian matrix. But there are some differences between them. Our truncation scheme is effective in the case of weak-coupling systems. In the strong-coupling systems, the partitions combined by the selected energetically favored partitions of H_1 and H_2 may be not energetically favored ones, while the discarded partitions can be energetically favored because of the strong interaction V_{12} between the combined two partitions. We can say that the scheme of Horoi *et al.* is more general, while our scheme is clearer in its physical picture. As we pointed out in Ref. [15], the weak-coupling scheme would be destroyed as the neutron number increases because the proton-neutron interaction between the partner orbital $\pi g_{9/2}$-$\nu g_{7/2}$ is strong. In this case, one should adopt the scheme of Horoi *et al.* or other effective way to truncate the configuration.

IV. SUMMARY AND CONCLUSIONS

Shell model calculations are carried out for nuclei with the $54\geqslant N\geqslant 50$ and $40\leqslant Z\leqslant 44$ using the partition truncation method; i.e., we first diagonalize the $N=50$ nuclei in a large model configuration space, then select out the dominate proton partitions to combine the neutron partitions to diagonalize the whole Hamiltonian. The calculated results are good in agreement with the experimental data. The concepts of independent nucleon-pair motion and homologous state structure proposed in analyzing the results in $A\sim150$ [15] and $A\sim208$ [14] are valid to explain the experimental and calculated results, which shows that the weak-coupling scheme is a very good approximation in shell model calculation for the midheavy and heavy nuclei where a full shell model calculation is difficult or even impossible. The success of this weak-coupling approximation combined with the above concepts applied to three different mass regions indicates that it is desirable and promising to apply this scheme to even midheavier and heavier nuclei. Furthermore, the weak-coupling scheme also provides us interesting pictures of the structure of midheavy and heavy nuclei, such as independent nucleon-pair motion and homologous structure.

ACKNOWLEDGMENTS

This work was supported in part by the National Natural Science Foundation, by the Doctoral Education Fund of the State Education Commission of China, and by the Research Fund of Nuclear Theory Center of HIRFL of China.

[1] D. H. Gloeckner and F. J. D. Serduke, Nucl. Phys. **A220**, 477 (1974).
[2] I. Talmi and I. Unna, Nucl. Phys. **19**, 225 (1960).
[3] S. Cohen, R. D. Lawson, M. H. Macfarlane, and M. Soda, Phys. Lett. **10**, 195 (1964).
[4] J. B. Ball, J. B. McGrory, and J. S. Larsen, Phys. Lett. **41B**, 581 (1972).
[5] Xiandong Ji and B. H. Wildenthal, Phys. Rev. C **37**, 1256 (1988).
[6] F. J. D. Serduke, R. D. Lawson, and D. H. Gloeckner, Nucl. Phys. **A256**, 45 (1976).
[7] R. Gross and A. Frenkel, Nucl. Phys. **A267**, 85 (1976).
[8] J. Blomqvist and L. Rydstrom, Phys. Scr. **31**, 31 (1985).
[9] H. Herndl and B. A. Brown, Nucl. Phys. **A627**, 35 (1997).
[10] J. Sinathas, L. D. Skouras, D. Strottman, and J. D. Vergados, J. Phys. G **18**, 1377 (1992).
[11] S. S. Ghugre and S. K. Datta, Phys. Rev. C **52**, 1881 (1995).
[12] B. Kharraja *et al.*, Phys. Rev. C **57**, 83 (1998).
[13] M. Horoi, B. A. Brown, and V. Zelevinsky, Phys. Rev. C **50**, R2274 (1995).
[14] Jin-nan Gu, A. Vitturi, Chang-hua Zhang, P. Guazzoni, L. Zetta, G. Graw, M. Jaskola, and G. Staudt, Phys. Rev. C **55**, 1 (1997).
[15] Chang-hua Zhang, Shun-jin Wang, and Jin-nan Gu, Phys. Rev. C **58**, 851 (1998).
[16] P. Guazzoni *et al.*, Z. Phys. A **356**, 381 (1997).
[17] B. A. Brown, A. Etchewgoyen, and W. D. M. Rae, Computer code OXBASH, MSU NSCL Report No. 524, 1984 (unpublished).
[18] R. D. Lawson, *Theory of the Nuclear Shell Model* (Clarendon, Oxford, 1980).
[19] A. Hosaka, K. I. Kubo, and H. Toki, Nucl. Phys. **A444**, 76 (1985).
[20] D. H. Gloeckner, Nucl. Phys. **A253**, 301 (1975).
[21] G. Audi and A. H. Wapstra, Nucl. Phys. **A565**, 1 (1993).
[22] Nucl. Data Sheets, electronic version http://www.nndc.bnl.gov
[23] C. M. Baglin, Nucl. Data Sheets **66**, 347 (1992).
[24] J. K. Tuli, Nucl. Data Sheets **66**, 1 (1992).
[25] L. K. Peter, Nucl. Data Sheets **68**, 165 (1993).
[26] Jin-nan Gu *et al.*, ''The structure of the high-excited special states in ^{206}Pb and ^{206}Tl'' report (unpublished).